https://doi.org/10.5194/egusphere-2022-291
Preprint. Discussion started: 10 May 2022

Climate Response to Severe Forestation: A Regional Climate Model Intercomparison Study

Olivier Asselin[1], Martin Leduc[1], Dominique Paquin[1], Katja Winger[2], Alejandro Di Luca[2], Melissa Bukovsky[3], Biljana Music[1], and Michel Giguère[1]

[1]Ouranos, Montréal, Québec, Canada
[2]Centre ESCER, Université du Québec à Montréal, Montréal, Québec, Canada
[3]National Center for Atmospheric Research, Boulder, Colorado

Correspondence: Olivier Asselin (asselin.olivier@ouranos.ca)

Abstract. The biogeophysical effects of severe forestation are quantified using a new ensemble of regional climate simulations over North America and Europe. Following the protocol outlined for the Land-Use and Climate Across Scales (LUCAS) intercomparison project, two sets of simulations are compared, FOREST and GRASS, which respectively represent worlds where all vegetation is replaced by trees and grasses. Three regional climate models were run over North America. One of them, the Canadian Regional Climate Model (CRCM5), was also run over Europe in an attempt to bridge results with the original LUCAS ensemble, which was confined to Europe. Overall, the CRCM5 response to forestation reveals strong inter-continental similarities, including a pronounced wintertime and springtime warming concentrated over snow-masking evergreen forests. Crucially, these northern evergreen needleleaf forests populate lower, hence sunnier latitudes in North America than in Europe. Snow masking reduces albedo similarly over both continents, but stronger insolation amplifies the net shortwave radiation and hence warming simulated over North America. In the summertime, CRCM5 produces a mixed response to forestation, with warming over northern needleleaf forests and cooling over southern broadleaf forests. The partitioning of the turbulent heat fluxes plays a major role in determining this response, but it is not robust across models over North America. Implications for the inter-continental transferability of the original LUCAS results are discussed.

1 Introduction

Afforestation and reforestation, herein combined as forestation, could remove significant amounts of carbon dioxide from the atmosphere (Roe et al., 2019; Shukla et al., 2019). Large-scale forestation, however, would also alter energy and water exchanges between the land and the atmosphere (Perugini et al., 2017). Turning grassland into forests, for instance, may lower albedo, increase surface roughness and facilitate the pumping of water from the soil to the atmosphere. These effects are collectively known as biogeophysical effects, in contrast to the biogeochemical effects pertaining to greenhouse gases and aerosol precursors (Pongratz et al., 2021). While forestation leads to biogeochemical cooling via carbon sequestration, biogeophysical effects may cause warming or cooling depending on a variety of factors such as latitude, time of year, tree species and original land cover (Duveiller et al., 2018b; Windisch et al., 2021). With forestation expected to contribute about

https://doi.org/10.5194/egusphere-2022-291
Preprint. Discussion started: 10 May 2022

a quarter of mitigation efforts pledged under the Paris agreement, it is essential that biophysical effects are quantified and accounted for.

The Land-Use and Climate, IDentification of Robust Impacts (LUCID) project was the first global climate model intercomparison effort aiming to quantify the biogeophysical effects of historical deforestation (Pitman et al., 2009; de Noblet-Ducoudré et al., 2012; Lejeune et al., 2017). While biogeophysical effects of historical deforestation were found to be modest when averaged over the globe, they could nevertheless match the magnitude of the more spatially diffuse biogeochemical effects at the regional scale. Yet, the biogeophysical effects of such land-use changes are not routinely included in regional climate model (RCM) intercomparisons (Mearns et al., 2012; Solman et al., 2013; Jacob et al., 2014). Numerous single-RCM studies have investigated the biogeophysical effects of land-use changes (Alexandru and Sushama, 2016; Mooney et al., 2020, 2021a; Bukovsky et al., 2021; Li et al., 2021), but the lack of a shared protocol makes comparison between models difficult.

The Land-Use and Climate Across Scales (LUCAS) intercomparison project was designed to improve the integration of land-use change in RCMs and to quantify their biogeophysical effects on climate. The first phase of LUCAS focuses on the biogeophysical effects of severe forestation in Europe using an ensemble of nine combinations of RCMs and land surface models (Davin et al., 2020). For every model combination, two sets of simulations are compared, FOREST and GRASS, respectively representing worlds where all vegetation is replaced with trees and grasses. This large simulation ensemble allowed investigations into various effects of forestation such as snow cover (Daloz et al., 2021; Mooney et al., 2021b), the diurnal air temperature cycle (Breil et al., 2020), the seasonal soil temperature cycle (Sofiadis et al., 2021), surface roughness and its role in the partition of turbulent heat fluxes (Breil et al., 2021), and the land-atmosphere coupling (Jach et al., 2020, 2022).

Are LUCAS findings specific to Europe, or may they be applicable to North America as well? To address this question, we apply the protocol designed for the original, European LUCAS initiative to a new set of RCMs and a new continent: North America. One of the ensemble members — the version 5 of the Canadian Regional Climate Model (CRCM5; Martynov et al. (2013); Šeparović et al. (2013)) — is also run over Europe. This allows to benchmark CRCM5 against other LUCAS members before proceeding with an intercomparison of the new simulation ensemble over North America. In the following section, the experiment setup is described in more detail. Then, CRCM5 simulations are compared over North America and Europe, providing a first look at the transferability of LUCAS findings to North America (section 3). In section 4, the robustness of the CRCM5 is assessed by comparing all three models of the present ensemble over North America. The various components of land-atmosphere energy fluxes are then averaged over the main forest families for both North America and Europe (section 5). Implications are discussed in section 6.

2 Experiment Setup

2.1 Model Ensemble

This paper presents simulations from three combinations of RCMs and land surface models, the main properties of which are outlined in table 1. The Weather and Research Forecast (WRF; Skamarock et al. (2005)) model version 3.5.1 is coupled to the Unified NOAH land surface model. Two versions of the Canadian Regional Climate Model (CRCM5 and CRCM6) are

https://doi.org/10.5194/egusphere-2022-291
Preprint. Discussion started: 10 May 2022

also employed, each coupled to a slightly different version of the Canadian Land Surface Scheme (CLASS; Verseghy (1991); Verseghy et al. (1993)). Differences between the two versions of CLASS — revised ponding depth over organic soils, revised snow albedo refreshment threshold and a new snow thermal conductivity algorithm — are modest in comparison to those between the CRCM5 and CRCM6 atmospheric components. The CRCMs are built on two different versions of the Global Environmental Multiscale Model dynamical core: 3.3.3.1 for CRCM5 (Côté et al., 1998) and 5.02 for CRCM6 (Girard et al., 2014). The physics packages, including radiation, convection and boundary layer schemes have also been updated significantly (McTaggart-Cowan et al., 2019).

Following Davin et al. (2020), all simulations presented here were performed at 0.44° ($\sim$ 50 km) horizontal resolution with lateral boundary conditions and sea-surface temperature driven by the 6-hourly ERA-Interim reanalysis (Dee et al., 2011). All three models were run over the North America CORDEX domain, and CRCM5 was run on the Europe CORDEX domain in addition (`https://cordex.org`). The simulations are analysed over 1986-2015, after a 7-year spin up allowing the models to adjust to land cover modifications.

2.2 Land Cover

Two simulations were performed for every member of the model-domain ensemble described above: FOREST and GRASS. The only difference between the two is land cover. For both sets of simulations, the vegetation distribution is based on Moderate Resolution Imaging Spectroradiometer (MODIS) land cover maps at 0.5° resolution (Lawrence and Chase, 2007). The MODIS maps are then modified according to the protocol outlined in Davin et al. (2020) to obtain the FOREST and GRASS land covers. In a nutshell, the FOREST experiment represents the theoretical maximum tree cover: the fractional cover of trees is expanded until trees fill all the area not occupied by bare ground, glaciers or lakes, which are left untouched. In the process, the proportion of the different tree families is kept fixed. Similarly, all vegetation is replaced by grassland in the GRASS experiment.

The model-dependent land categories used in the conversion are outlined in table 1. Although the MODIS data is projected onto multiple tree categories in both NOAH and CLASS, two classes dominate (bold in table 1): deciduous broadleaf trees and evergreen needleleaf trees. Other tree categories appear (italicized in table 1), but they play a minor role such that we neglect them in the analysis. For the GRASS experiment, all MODIS grasses project onto a single land category. The main properties of these dominant tree and grass categories, which differ between CLASS and NOAH, are outlined in table 2.

Figure 1 displays the fraction of land occupied by broadleaf and needleleaf trees (left and center panels) in the FOREST experiment, the sum of which gives the grass cover from the GRASS experiment (right panels). The non-grass fraction of the right panels is either covered by deserts, glaciers or lakes. The FOREST versions of North America and Europe reveal a similar pattern: needleleaf forests tend to concentrate at higher latitudes and broadleaf forests at lower latitudes. One difference that will prove important, however, is that these forests appear at lower, hence sunnier latitudes in North America. In eastern Canada, for instance, latitudes 45° to 55° — from the Great Lakes up to Northern Quebec — are densely populated by needleleaf trees in the FOREST world. By comparison, needleleaf trees reach complete coverage only north of 60° in eastern Europe. Broadleaf forests extend from the Mediterranean region at around 40° up to 55° in Europe, while they are mostly concentrated between

https://doi.org/10.5194/egusphere-2022-291
Preprint. Discussion started: 10 May 2022

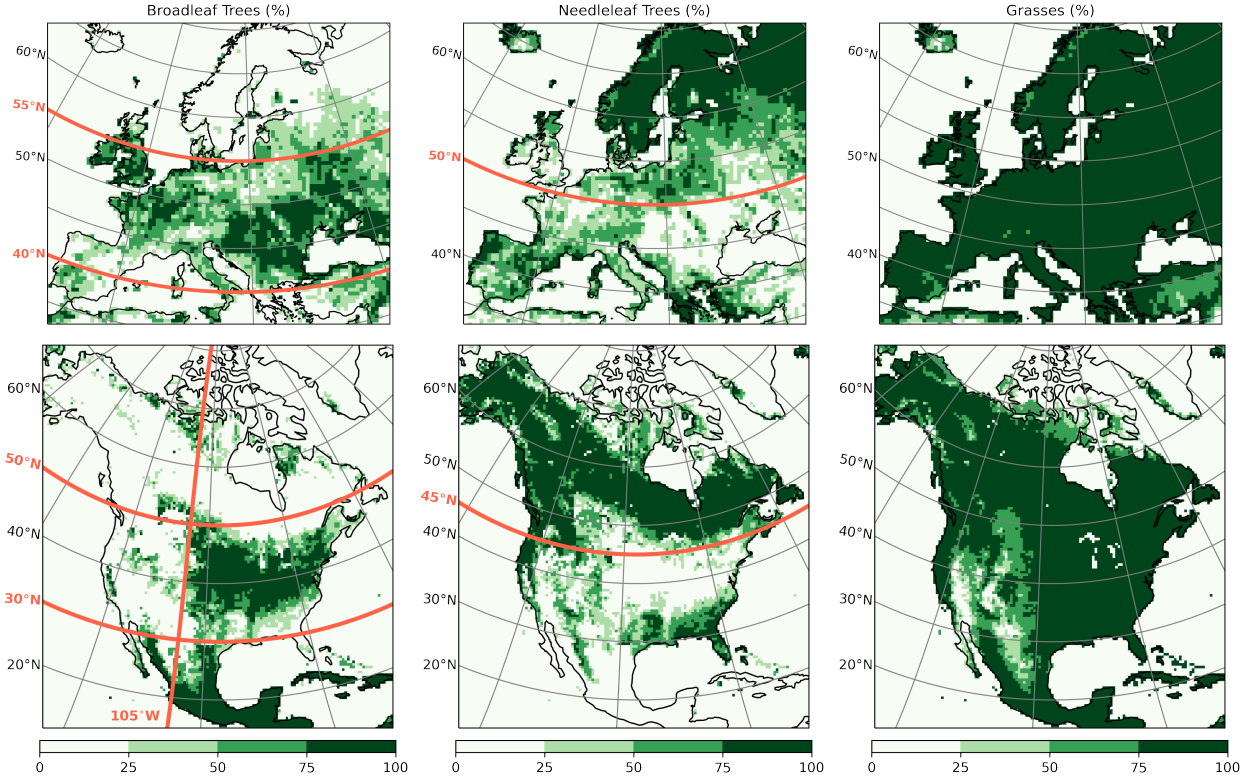

Figure 1. Vegetation fraction (%) of the plant functional types considered in this experiment. The left and center panels are the tree types present in the FOREST experiment, the sum of which gives the grasses fraction in the GRASS experiment, shown in the right panels. Non-grass cover in the right panels is either water, glaciers or bare soil. The orange longitude and latitudes lines delimit the two main forest family considered: southern broadleaf and northern needleleaf forests. A longitude-latitude coordinate is considered part of the given forest if it falls between these boundaries and its type accounts for more than 50% of the vegetation fraction.

30° and 45° at most in North America. (We do not include the tropical region in the analysis for it is too close from the domain boundary.)

For subsequent analysis, we define two main forests families: northern needleleaf and southern broadleaf forests. In figure 1, these forests are delimited by the colored latitudinal and longitude lines. A grid point is considered part of a given forest if it falls between these boundaries and its type accounts for more than 50% of the vegetation fraction. For instance, any grid point of America north of 30°N, south of 50°N and east of 105°W with more than 50% broadleaf tree cover is considered part of the southern broadleaf forest.

https://doi.org/10.5194/egusphere-2022-291
Preprint. Discussion started: 10 May 2022

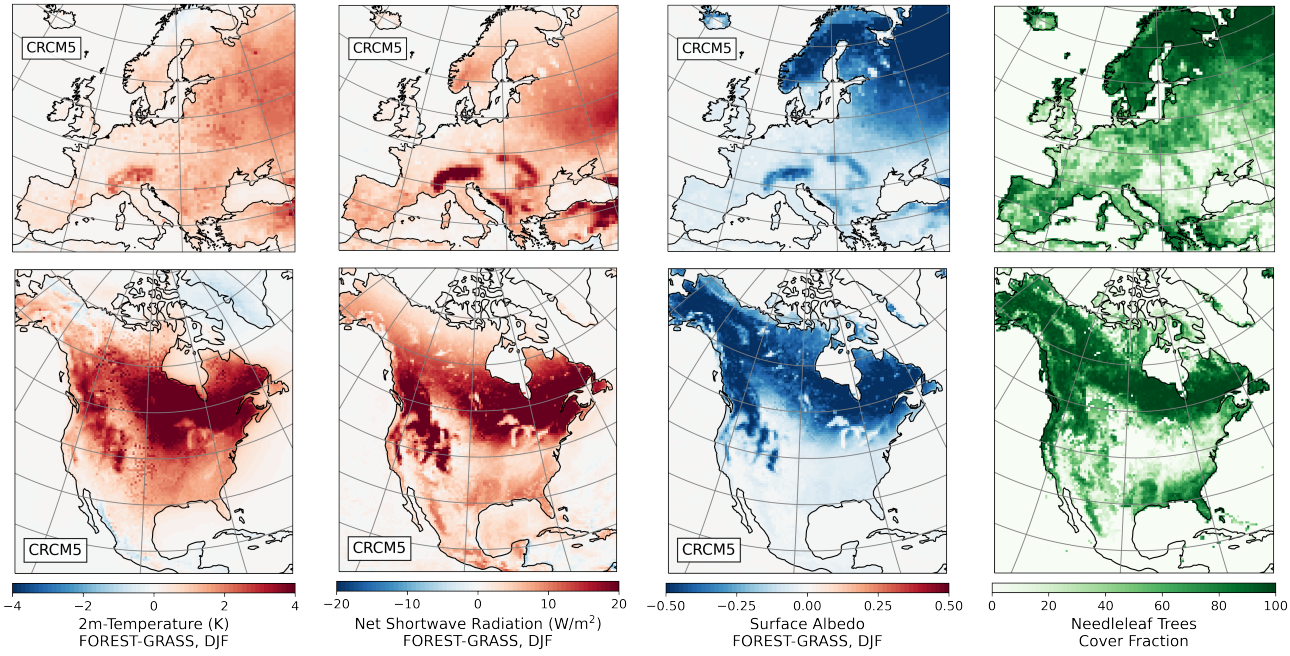

Figure 2. CRCM5-CLASS wintertime response to forestation (FOREST-GRASS) averaged over 1986-2015, DJF. From left to right: near-surface temperature, shortwave radiation excess, surface shortwave albedo and needleleaf tree distribution.

3 CRCM5 over North America and Europe

We begin with an analysis of the CRCM5-CLASS simulations over North America and Europe. This provides an opportunity for comparing the response to forestation over two different continents, and thus investigate whether the findings from the original, European LUCAS study may apply to North America. We analyse the responses for wintertime and summertime because they capture the main biogeophysical effects of forestation and provide a blueprint for the more thorough analysis of section 4. To highlight the effects of forestation, all figures in this section display the difference between the afforested and deforested climatologies, *i.e.* FOREST minus GRASS.

3.1 Winter

The CRCM5 winter response to forestation is summarized in figure 2. In both Europe and North America, forestation causes a widespread wintertime warming peaking at mid-high latitudes. This warming pattern matches net downwelling shortwave radiation, suggesting that solar energy absorption dominates the temperature signal. Indeed, high-latitude evergreen needleleaf forests are collocated with a strong drop in the shortwave albedo. In CLASS, these trees can intercept snow on their canopy, which increases their albedo. But snow coverage remains incomplete, and the dark canopy of needleleaf trees can mask snow

https://doi.org/10.5194/egusphere-2022-291
Preprint. Discussion started: 10 May 2022

on the ground. By contrast, grasses may be fully buried by snow. Therefore, snow-covered evergreen forests absorb a much higher fraction of the incoming shortwave radiation than snow-buried grasses, causing warming.

Snow masking was also found to cause wintertime warming in the original LUCAS experiment (Davin et al., 2020). Like CRCM5, all LUCAS members simulate a drop in albedo resulting in warming over the northern evergreen needleleaf forests of Europe (figure 1 of Davin et al. (2020)). We note, however, that CRCM5 has the strongest temperature response of the LUCAS ensemble (see figure S1). In other words, the wintertime warming mechanism seems robust across models and continents, but one must keep in mind that CRCM5-CLASS may be among the most sensitive to it.

While snow masking is well known and documented in both observational (Li et al., 2015; Duveiller et al., 2018b) and modeling studies (Betts, 2000; Davin et al., 2020), a more overlooked fact is that its warming effect depends on the strength of insolation, hence on latitude and time of year. Given a fixed drop in albedo from snow masking, net shortwave radiation and warming will be larger where and when there is more incoming sunlight. In figure 2, the albedo drop is uniform over the dense northern needleleaf trees, but the shortwave radiation excess and warming responses decay with increasing latitude. The warming response is strongest at the lowest latitudes where dense evergreen forests are covered by snow. This explains why the shortwave excess and the accompanying warming response are much stronger and longitudinally widespread in North America than in Europe. Dense evergreen needleleaf forests populate broader swaths and lower latitudes in North America (figure 1). Snow masking by needleleaf trees have the same effect on albedo on both continents, but the resulting shortwave radiation excess and hence warming is much stronger over the sunnier, lower-latitude North American forests.

3.2 Summer

The temperature response is more complex during summer than winter. In both North America and Europe, forestation produces a dipole-like response, with a warming over northern needleleaf forests and a mild cooling over southern broadleaf forests (figure 3). The response is cooler overall in Europe.

Over northern needleleaf forests, warming regions coincide with a shortwave radiation excess, itself caused by various factors. Firstly, forests — especially needleleaf forests — are darker than grasses. Secondly, the warmer FOREST climate is consistent with precocious snow melt at high latitudes, especially in North America (see section 4). These two effects significantly lower albedo, and thus increase solar energy input at high latitudes. Thirdly, there is a noticeable drop in cloud cover over northern Canada (figure 4), further increasing incoming solar radiation and hence the warming in this region.

Over the dense lower-latitude broadleaf forests, heavy transpiration instead causes increased cloud cover, which significantly reduces incoming shortwave radiation in central Europe and the Eastern US (figure 4). The cooling spots, however, cannot be fully explained by the weaker, but still positive, net downwelling shortwave radiation. Differences in the partitioning of turbulent heat fluxes play a dominant role in these regions. A useful way to capture these changes is the evaporative fraction (EF):

$$\mathrm{EF} = \frac{\mathrm{LH}}{\mathrm{LH} + \mathrm{SH}}, \tag{1}$$

https://doi.org/10.5194/egusphere-2022-291
Preprint. Discussion started: 10 May 2022

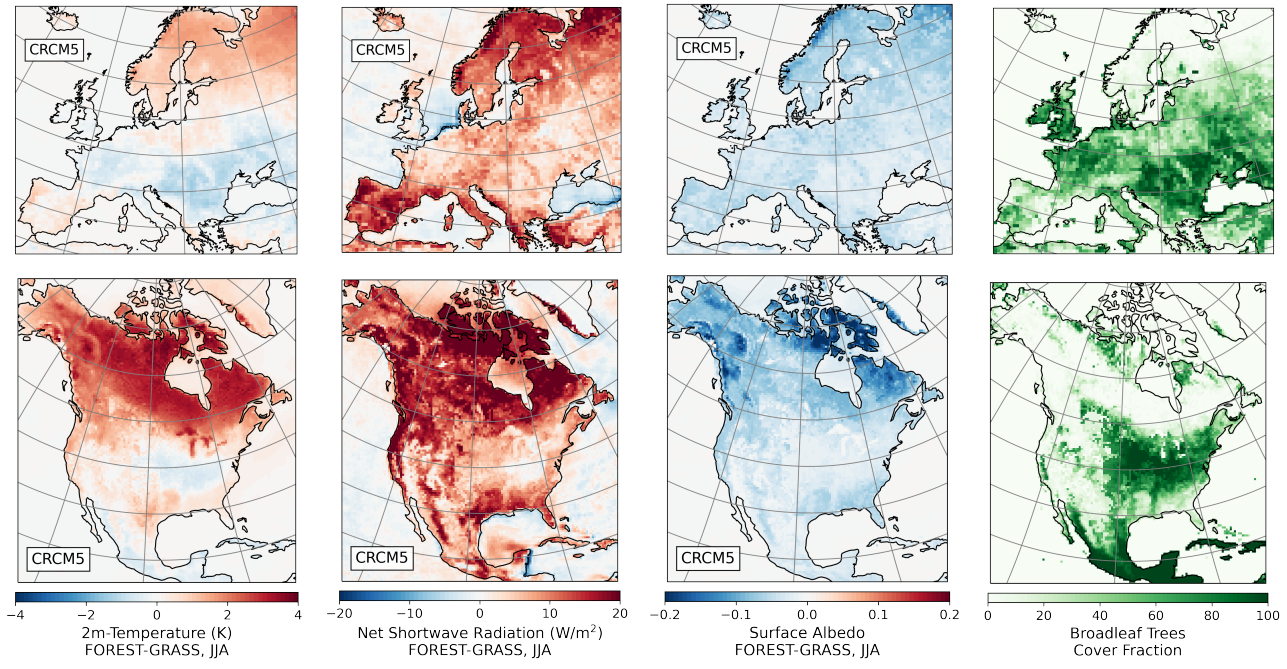

Figure 3. CRCM5-CLASS summertime response to forestation (FOREST-GRASS) averaged over 1986-2015, JJA. From left to right: near-surface temperature, shortwave radiation excess, albedo and broadleaf tree distribution.

where LH and SH are the latent and sensible heat fluxes. That is, EF represents the fraction of turbulent fluxes due to evapotranspiration.

Comparing figures 3 and 4 reveals a significant negative correlation between temperature and EF. Moreover, regions of increasing (decreasing) EF tend to match the location of broadleaf (needleleaf) forests. Mature, unstressed summertime broadleaf trees, with their deeper roots, denser foliage and weaker stomatal resistance, are more efficient at intercepting rain and pumping water from the soil than needleleaf trees — at least in CLASS (see parameters used in table 2). As such, broadleaf forests are prone to giving away more of their energy via evapotranspiration than via sensible heat fluxes, leading to a relative cooling of near-surface air. The opposite is true of needleleaf forests: these regions undergo less evaporative cooling, instead giving away more of their energy via sensible heat fluxes, causing near-surface air warming. Satellite-based data also suggests that converting grasses to needleleaf (broadleaf) forests increases sensible (latent) heat fluxes significantly (Duveiller et al., 2018b).

Changes in EF are related to significant alterations of the summertime water budget (figure 4; wintertime changes are negligible in comparison). Overall, forestation leads to enhanced evapotranspiration, especially over broadleaf forests. Precipitations are also increased, with comparable contributions from stratiform and convective forms (not shown). In relative terms, FOREST simulations can produce more than a 50% increase in precipitations compared with the GRASS simulations (not shown). Changes are most drastic over Europe, where dense broadleaf forests occupy a broader swath of the continent and deserts are

https://doi.org/10.5194/egusphere-2022-291
Preprint. Discussion started: 10 May 2022

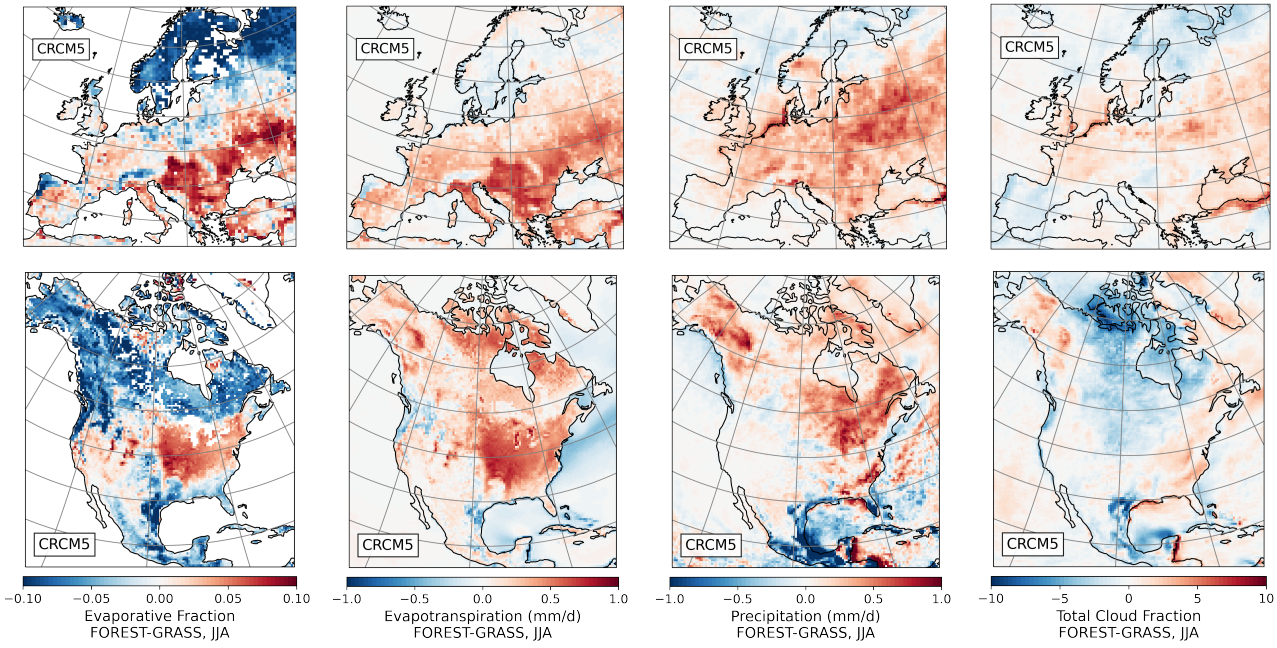

Figure 4. Summertime water budget response to forestation for CRCM5-CLASS. From left to right: evaporative fraction (1), evapotranspiration, precipitation changes, and cloud cover.

rarer (figure 1). One also notes that the response patterns of evapotranspiration, precipitations and cloud coverage tend to be collocated in space.

The CRCM5-LUCAS comparison for summer is challenging. In the original LUCAS experiment of Davin et al. (2020), the model ensemble exhibits a wildly divergent summertime temperature response to forestation, including widespread cooling and warming (see their figure 2). Interestingly, the multi-model mean of the LUCAS models is a warming-cooling north-south dipole pattern akin to the CRCM5 response, albeit with weaker amplitude. While this shows that CRCM5 sits well within the LUCAS summertime uncertainty range, it is unclear how one should interpret the mean from such divergent data.

We also note that one of the nine LUCAS members, CCLM-CLM4.5 (short for the COSMO Climate Limited-area Community RCM coupled to the Community Land Model), responds similarly to CRCM5 in summertime. Both models produce a north-south temperature dipole associated with an inverted EF dipole (see figure S2). In other words, in both models southern broadleaf forests favor latent over sensible heat fluxes, and vice versa for northern needleleaf forests. It is unclear, however, what one can learn from this similarity, as two other regional climate models (RegCM and WRF) were coupled to the same land model and yet did not produce a dipole temperature response.

The above remark nevertheless illustrates one of the more robust features across both LUCAS and the present study: the partition of turbulent fluxes plays a major role in determining the summertime temperature response. In their figure 11, Davin et al. (2020) show that a decreased EF is associated with warming (and vice versa) for all models during summertime Scandi-

https://doi.org/10.5194/egusphere-2022-291
Preprint. Discussion started: 10 May 2022

navia. The same is true of CRCM5 on both continents: compare the temperature and EF summertime maps from our figures 3 and 4. While the link between EF and temperature responses is robust, the origin of the inter-model divergence in the partition of turbulent fluxes remains illusive despite considerable efforts (Pitman et al., 2009; de Noblet-Ducoudré et al., 2012).

These difficulties should not obscure the encouraging implications of the present section. The broad similarity between the CRCM5 responses over North America and Europe suggests that the more robust results from the original LUCAS experiment in Europe may be transferable to North America after correcting for differences in the vegetation distribution (further discussed in section 6). We also found that the CRCM5 response to forestation sits well within the LUCAS ensemble, with a similar wintertime warming due to snow masking (albeit on the stronger end of the spectrum) and a mixed summertime temperature response largely driven by the partition of turbulent fluxes. This provides confidence regarding the relative skill of CRCM5-CLASS in simulating the main physical processes implicated in the biogeophysical response to forestation. In the following section, CRCM5-CLASS will provide a useful basis for comparing the forestation response in North America of two other models, CRCM6-CLASS and WRF-NOAH.

4 Model Intercomparison over North America

One of the main takeaways from earlier model intercomparison studies of land-use change — such as LUCID and LUCAS — is that model intercomparison is crucial indeed. This study does not differ: the response to forestation shows strong inter-model divergence. One cannot pick a single model and hope for an accurate picture of the effects of land-use change. In what follows, all three combinations of regional climate and land surface models (table 1) are compared over North America. Overall, WRF-NOAH produces a widly different response to the CRCMs, which have relatively similar responses in comparison. Still, despite sharing the same land surface model and parameters, there are nontrivial and interesting differences between CRCM5 and CRCM6.

4.1 Winter

Mass afforestation causes widespread winter warming in all models (figure 5). The CRCMs display a similar warming pattern reaching peak intensity at mid-high latitudes, consistent with the snow-masking albedo effect of evergreen needleleaf forests (see section 3.1). By comparison, WRF's response is milder and peaks at lower latitudes.

The shortwave radiation budgets of WRF and CRCMs help explain the source of this temperature difference. WRF shows no shortwave radiation response to forestation at snow-covered high latitudes, whereas the CRCMs may produce upwards of 20 W/m^2 excess in these regions. This is because there is essentially no snow-making effect in NOAH at high latitudes: snow fully hides the forest cover as soon as it reaches a depth of 8 cm (or 4 cm for grass). The albedo values of snow are used wherever the snow pack depth is above this threshold, *i.e.* over most of Canada in wintertime. There is thus no albedo difference between FOREST and GRASS simulations at high-latitudes for WRF.

Instead, the WRF winter warming maximum aligns with an albedo drop in the prairies and US midwest. In this region, the snowpack depth crosses the WRF snow cover threshold, which is higher for the afforested world. This creates a warming

https://doi.org/10.5194/egusphere-2022-291
Preprint. Discussion started: 10 May 2022

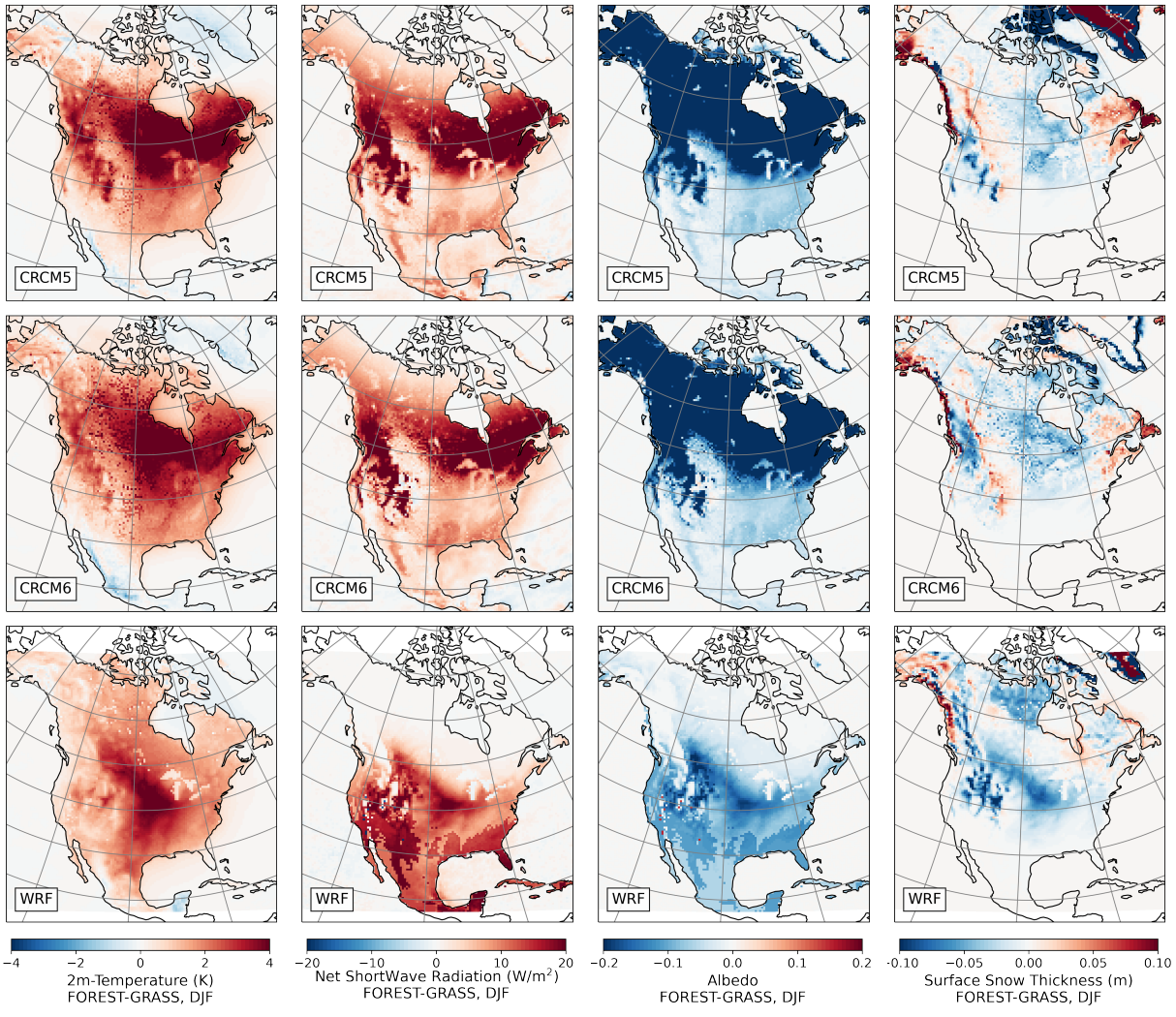

Figure 5. Most relevant wintertime (DJF) variables: near-surface temperature, excess shortwave radiation, albedo and snow depth. All panels show the differences between FOREST and GRASS simulations.

feedback whereby the lower albedo of forests increases net shortwave radiation, causing warming and inhibiting the formation of a deep snow pack.

4.2 Spring

Forestation causes the strongest warming response during springtime in the CRCMs (figure 6). Like in winter, the snow-masking albedo effect dominates the signal, but its impact on shortwave radiation excess and hence temperature is supercharged

https://doi.org/10.5194/egusphere-2022-291
Preprint. Discussion started: 10 May 2022

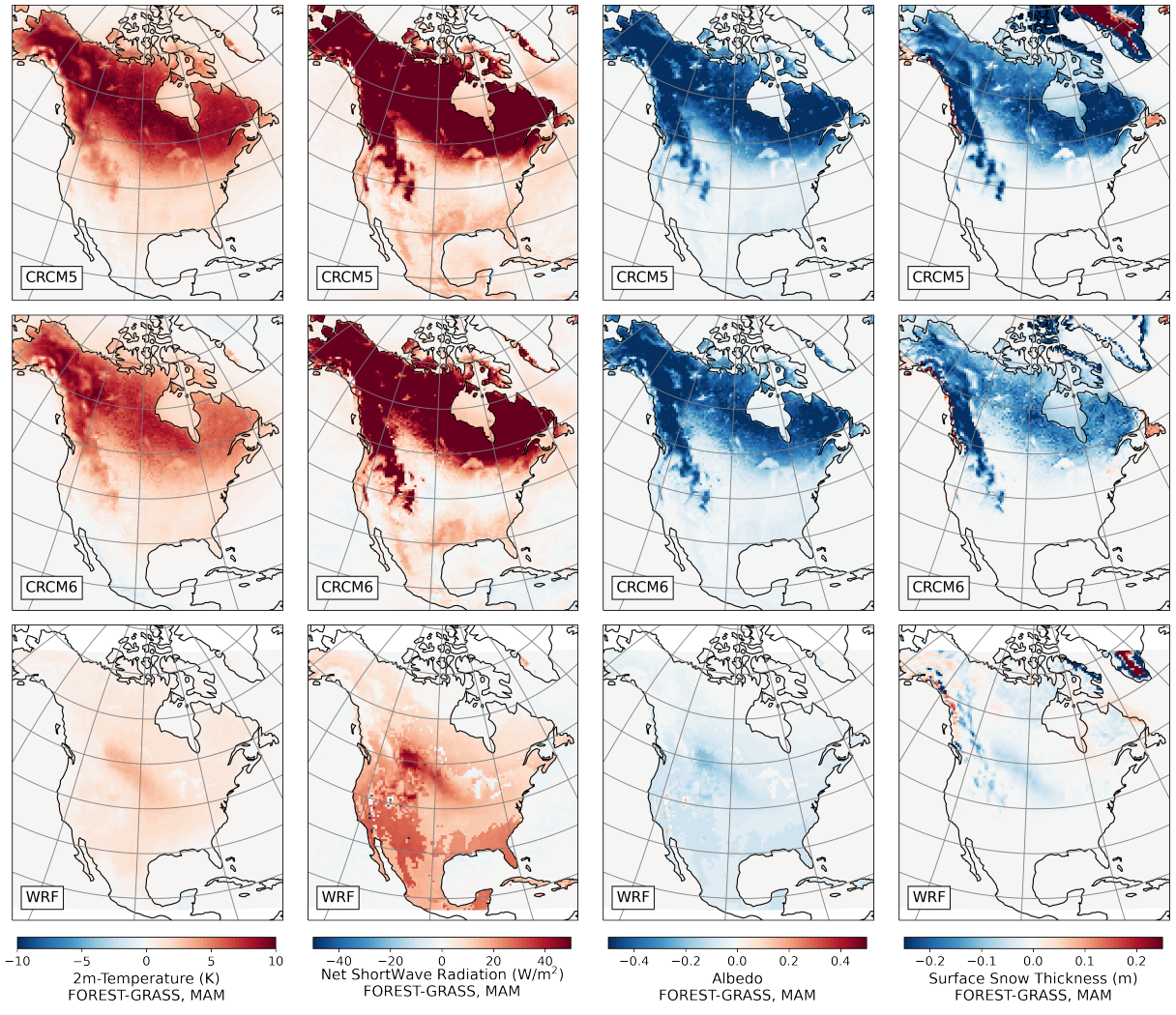

Figure 6. Same as figure 5 but for spring (MAM): near-surface temperature, excess shortwave radiation, albedo and snow depth. Compared with figure 5, all colorbars have been scaled up by a factor of 2.5 to avoid complete saturation. All panels show the differences between FOREST and GRASS simulations.

by the much stronger springtime insolation. In figure 6, all colorbars have been scaled up by 250% compared with the winter-
210 time figure 5 to avoid complete saturation. Importantly, the magnitude of the albedo drop is similar for spring and winter. But in spring, the impact on shortwave radiation excess and hence temperature is amplified and extended to much higher latitudes. This echoes a point made in section 3.1: the impact of the snow-masking effect on temperature depends on insolation, which itself depends strongly on latitude and time of the year. The more sunlight there is, the more potent this effect becomes.

https://doi.org/10.5194/egusphere-2022-291
Preprint. Discussion started: 10 May 2022

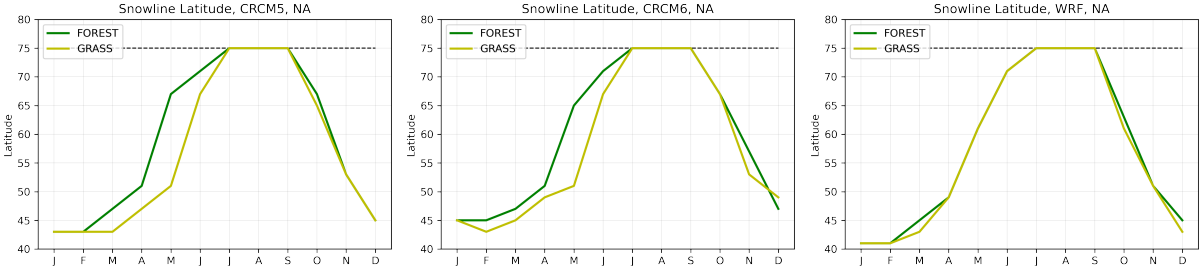

Figure 7. Latitude of the snowline as a function of the month, averaged over 1986-2015. The snowline latitude is defined as the lowest latitude for which over 50% of the land tiles are covered by at least 10 cm of snow. Greenland was removed from this calculation, and the snowline latitude was capped at 75° (dashed line).

The springtime warming response to forestation happens in concert with precocious snow melt. Figure 7 shows the annual cycle of snow line latitude in the FOREST and GRASS simulations. Consistent with LUCAS (Mooney et al., 2021b), in CRCMs forestation causes a large reduction in snow cover during the melting period, but little impact during the accumulation phase.

4.3 Summer

Compared with the strong summertime warming-cooling dipole produced by the CRCMs, WRF exhibits a significantly milder and more uniform warming response (figure 8). This large inter-model divergence in temperature is not, as in winter and spring, mainly captured by the albedo-driven shortwave radiation excess. Summertime turbulent fluxes have a magnitude similar to radiative fluxes, and they also strongly diverge between models (see figure 9).

Let's begin with what all models agree on. Forests are darker than grasses (table 2), such that albedo is lowered by forestation (figure 8). The albedo drop is compounded by precocious snow melt over northern Canada in the warmer afforested worlds simulated by the CRCMs. Cloud effects aside, the albedo drop causes an increase in net downwelling shortwave radiation, and thus in the amount of energy available to warm the surface. All models also agree that trees increase the surface roughness (table 2), thereby facilitating energy transfer back to the atmosphere as turbulent heat fluxes. Indeed, total turbulent fluxes are enhanced almost everywhere by forestation (see figure 9).

Models diverge strongly, however, in how turbulent heat fluxes are partitioned between their sensible and latent components. Differences in the vegetation parameters (table 2) can explain some of this divergence, because they influence the evapotranspiration efficiency of the surface. If vegetation is poor at intercepting rain or pumping water from the soil, sensible heat fluxes will likely dominate and transfer heat via convection. In the summertime, the surface is typically warmer than the air above such that sensible heat fluxes warm the atmosphere. If vegetation favors rain interception and re-evaporation, or if it has low canopy resistance and can easily access water in the soil, latent heat fluxes may take over sensible heat fluxes and cause near-surface cooling.

https://doi.org/10.5194/egusphere-2022-291
Preprint. Discussion started: 10 May 2022

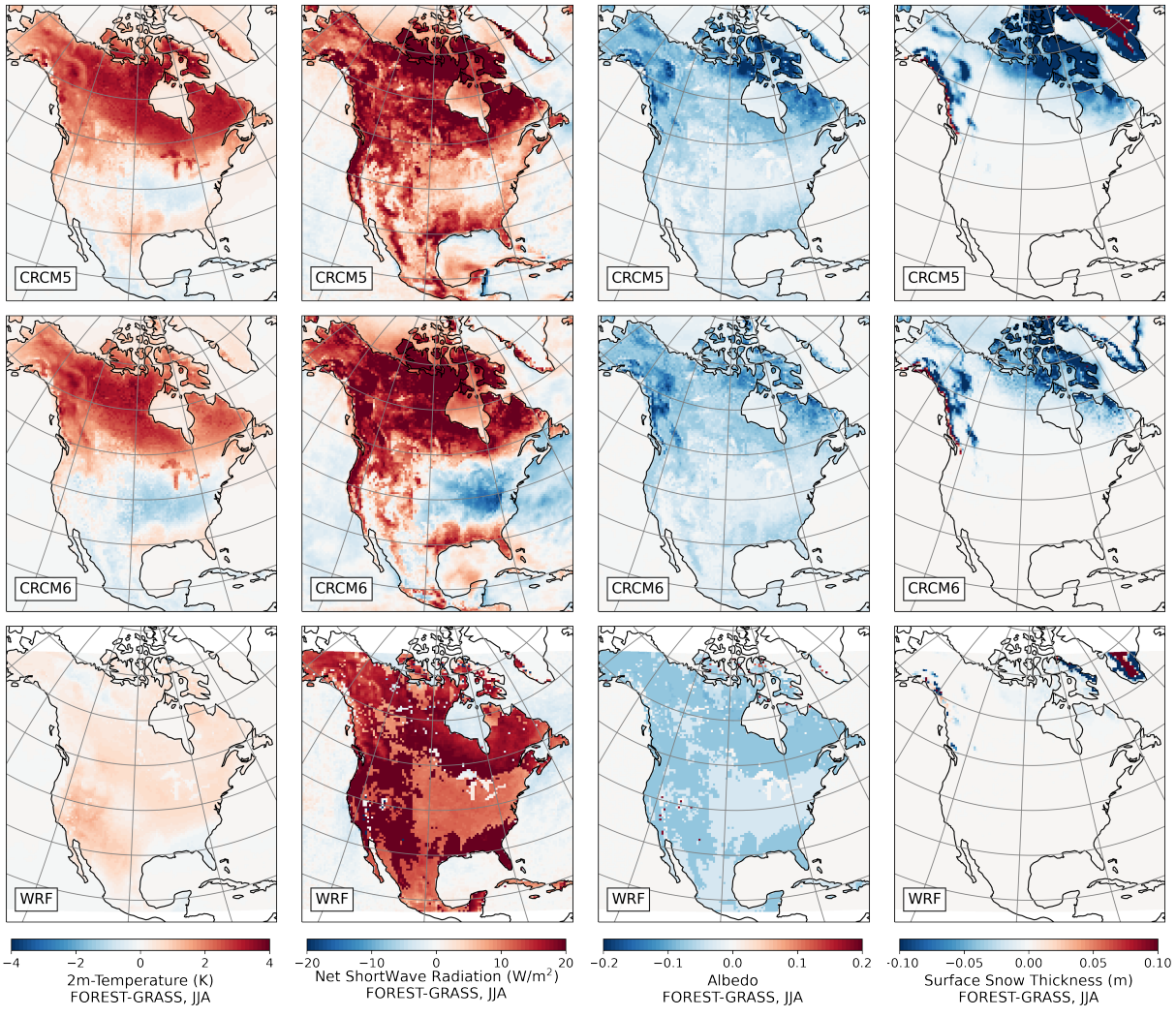

Figure 8. Same as figure 5 but for summer (JJA): near-surface temperature, excess shortwave radiation, albedo and snow depth. All panels show the differences between FOREST and GRASS simulations.

The evapotranspiration efficiency of the dominant plant functional types varies strongly between NOAH and CLASS (table 2). CLASS broadleaf trees, with the deepest roots, lowest stomatal resistance and highest roughness length of all vegetation categories, favor transpiration more than needleleaf trees or grasses. They also have the highest maximum leaf area index, making them great at intercepting rain during summer, such that more precipitation re-evaporates before reaching the ground. Over eastern US broadleaf forests, CRCMs thus simulate a strong increase of the evaporative fraction, leading to a relative cooling of the near-surface air (figure 9). In NOAH, needleleaf trees appear to favor evapotranspiration more than both broadleaf trees and grasses. Despite their higher minimum stomatal resistance, they have the deepest roots, and the highest roughness

https://doi.org/10.5194/egusphere-2022-291
Preprint. Discussion started: 10 May 2022

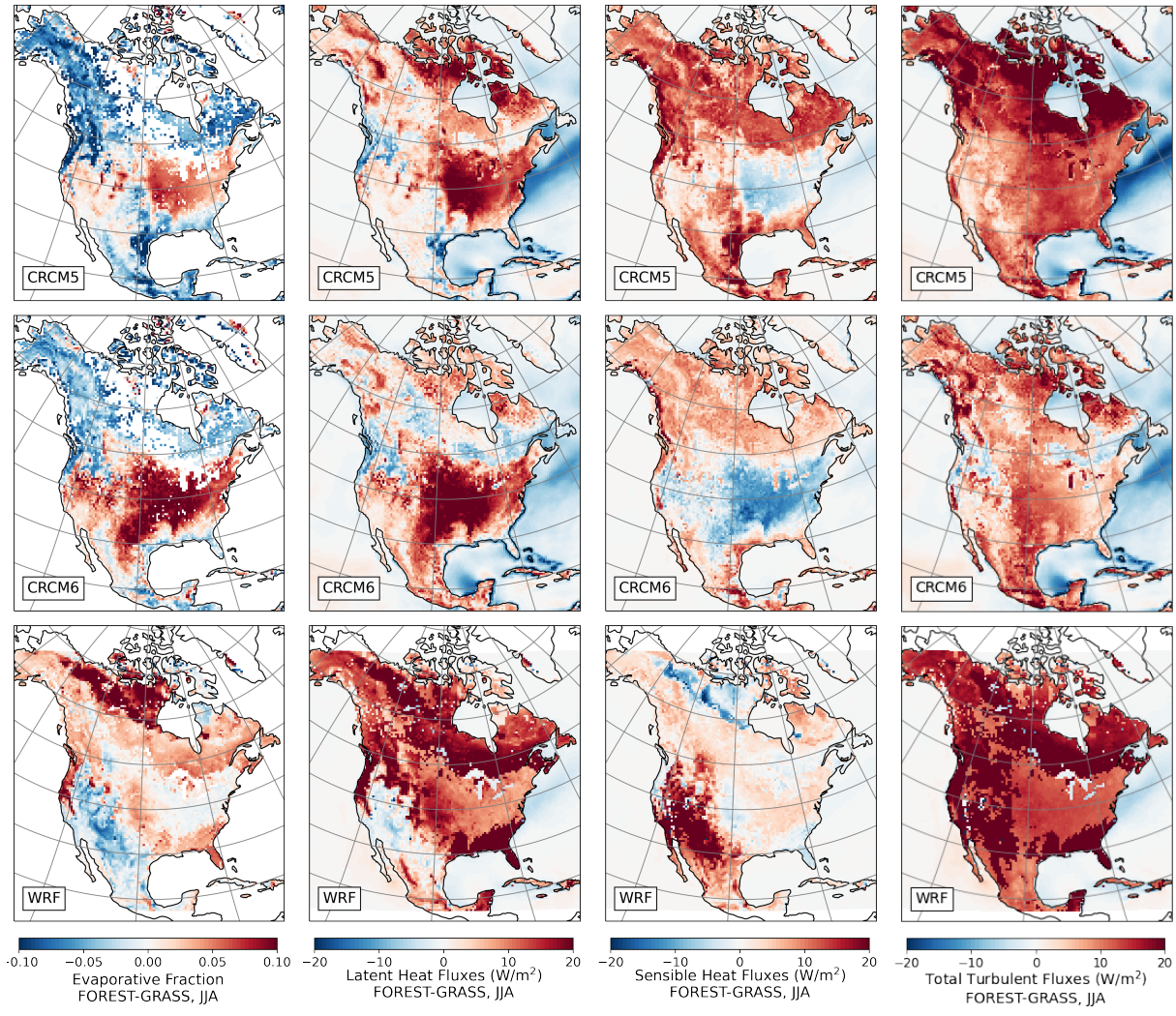

Figure 9. Summertime turbulent heat fluxes: evaporative fraction (defined in equation 1), latent heat, sensible heat and their sum. All fluxes are defined as positive when pointing upwards.

and leaf area index. As such, there is an increase of evaporative fraction and cooling over southeastern US needleleaf forests. In water-stressed regions such as southwest US, however, a dominance of sensible heat fluxes results in warming (figure 9).

245 The partition of turbulent fluxes may also significantly alter the radiative fluxes. Strong latent heat fluxes can stimulate cloud formation, which blocks incoming sunlight, thereby reducing the amount of energy available to warm the surface. This coupling is particularly prominent in CRCM6, in which southern broadleaf forests favor high evapotranspiration rates, generating

https://doi.org/10.5194/egusphere-2022-291
Preprint. Discussion started: 10 May 2022

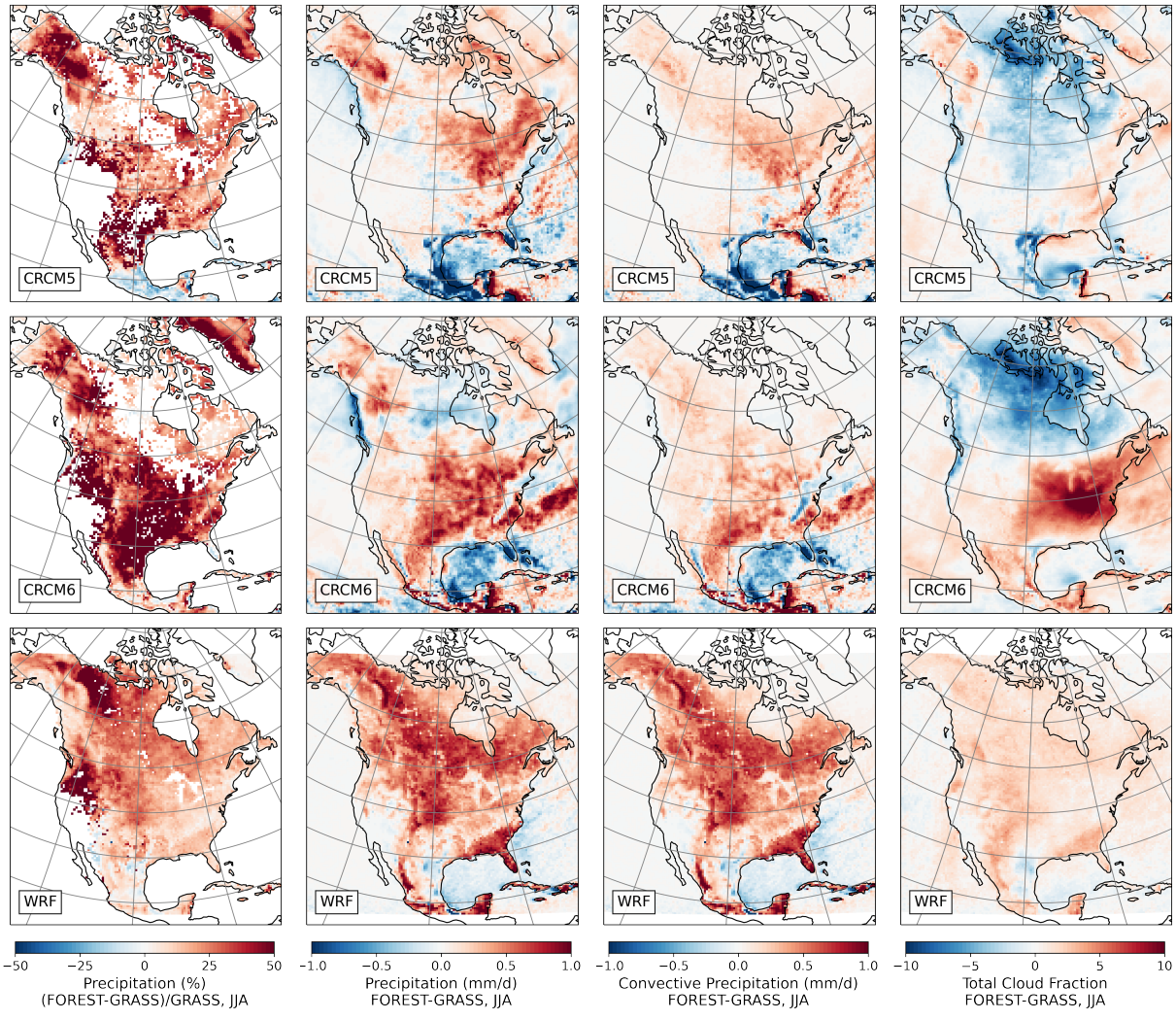

Figure 10. Summertime precipitation and cloudiness. The leftmost panels show the relative change in precipitation (pr) from forestation, namely $100\% \times (\mathrm{pr}_{\mathrm{FOREST}} - \mathrm{pr}_{\mathrm{GRASS}})/\mathrm{pr}_{\mathrm{GRASS}}$. The other panels show the conventional FOREST minus GRASS absolute changes for total precipitation (convective plus stratiform), convective precipitation and cloud fraction.

stronger precipitation and cloud coverage (figure 10), which drastically reduces incoming shortwave radiation (figure 8). The net result is a strong cooling of the surface.

250 The evaporation-precipitation feedback described above shows that one cannot fully explain the partitioning of turbulent fluxes from the parameters of table 2 alone. CRCM5 and CRCM6 share the same land surface model and parameters, yet produce different turbulent heat fluxes (figure 9), which in turn feedback on radiative fluxes and temperature (figure 8). In this

https://doi.org/10.5194/egusphere-2022-291
Preprint. Discussion started: 10 May 2022

particular case, it is plausible that the changes in the parameterizations of boundary layer and convective processes bear some of the responsibility for the divergence observed (table 1).

4.4 Fall

Forestation has the weakest temperature response during fall (figure 11). Unlike winter and spring, the snowpack is confined to very high latitudes. Even if snow-masking in CRCMs produces a noticeable albedo drop in Alaska and Northern Canada, the effect on shortwave radiation excess and hence temperature is mild because of weak insolation at those latitudes. Thus, the snow-masking albedo effect that fueled the wintertime and springtime responses is rather weak during fall. Similarly, the dark canopy of northern needleleaf forests does not cause as much warming as in summertime because of comparatively weaker insolation.

The largest evapotranspiration rates that made the southern summertime response so dynamic is also weaker during fall, as deciduous trees lose their foliage. A mild cooling is nevertheless apparent over the eastern US forests. As in summertime, enhanced cloudiness reduces incoming sunlight in CRCMs (not shown).

5 Energy Fluxes over Needleleaf and Broadleaf Forests

Most of the maps shown so far reveal patterns resembling the vegetation distribution. In particular, the two main forest families identified earlier in figure 1 — northern needleleaf and southern broadleaf forests — behave in markedly distinct ways. In what follows, the various components of the surface-atmosphere energy fluxes are spatially averaged over these two main forests for both continents, providing a complementary overview on the biogeophysical effects of forestation.

5.1 Northern Needleleaf Forests

Evergreen needleleaf forests are darker than grasses (table 2), hence absorb more shortwave radiation. Both the surface and near-surface air warm up in response. This is true for all seasons, models and continents presented here (figure 12). Davin et al. (2020) produced a similar energy breakdown over Scandinavia (their figure 9), which loosely fits our northern needleleaf forest region in Europe (figure 1). They also find forestation to generate excess shortwave radiation and near-surface warming in all models for winter and spring, and for most, but not all models, in summer and fall.

Figure 12 also reveals weak seasonality in how evergreen needleleaf forests spend their excess energy. That is, the breakdown of fluxes for a given model is similar across seasons after scaling for net downwelling shortwave radiation. The one main exception is the WRF-NOAH needleleaf forest, which evacuates most of its shortwave excess energy through latent heat fluxes. Because of this, northern needleleaf forests generate almost no warming (figures 8 and 12). By contrast, CRCM-CLASS needleleaf trees have a similar response all year round, and favor sensible heat fluxes more than they do latent heat fluxes. As such, these forests spend their excess shortwave energy in a way that causes unabated warming.

While the ratios of the various energy flux components undergo little seasonal variation, the magnitude of the springtime response is outstanding. In figure 12 the temperature and energy fluxes scales have respectively been scaled up by factors of

https://doi.org/10.5194/egusphere-2022-291
Preprint. Discussion started: 10 May 2022

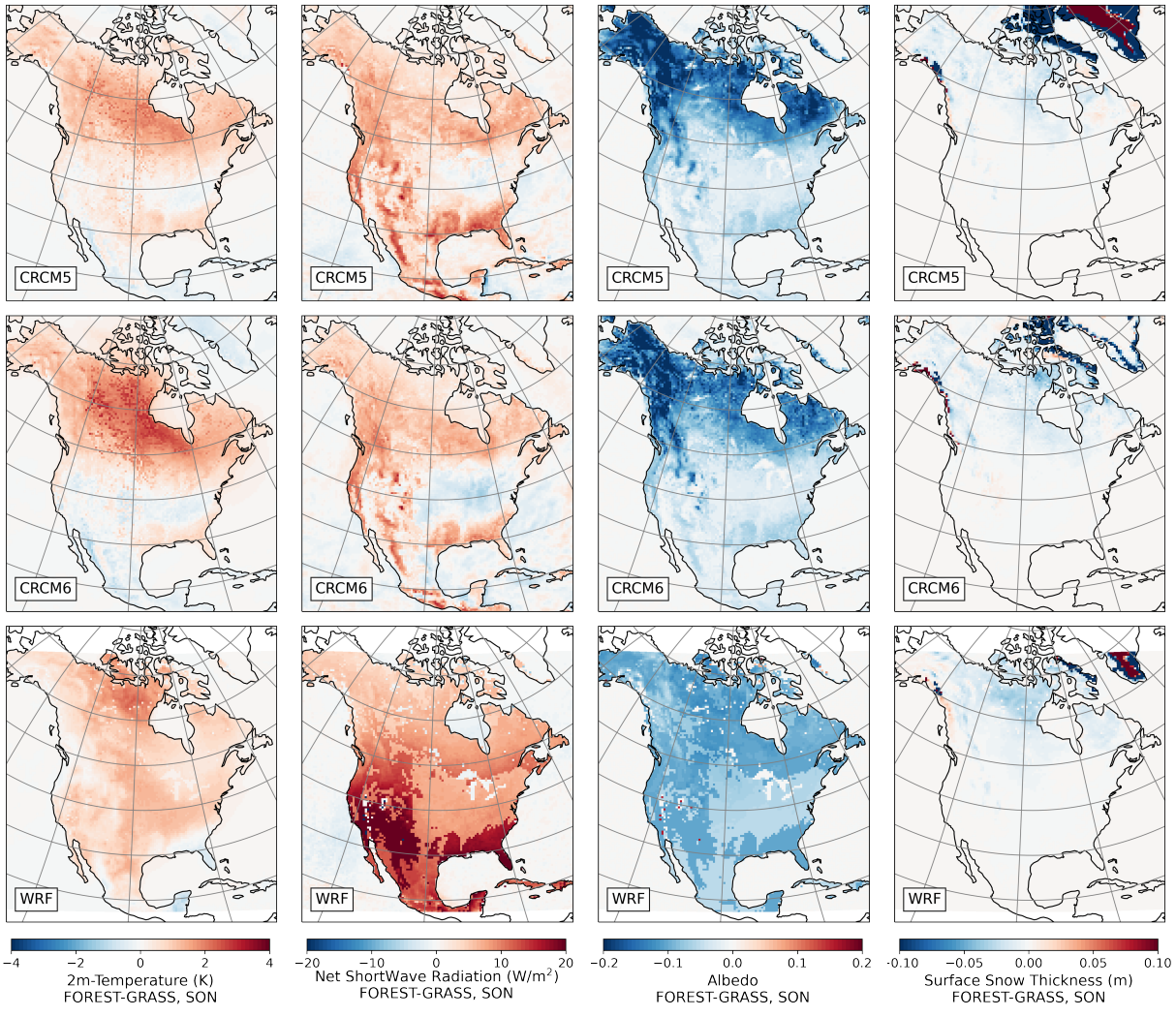

Figure 11. Same as figure 5 but for fall (SON): near-surface temperature, excess shortwave radiation, albedo and snow depth. All panels show the differences between FOREST and GRASS simulations.

2.5 and 5 to avoid overshoot. Compared with winter, springtime insolation is much greater at high latitudes such that the large albedo drop from snow-masking produces a stronger shortwave radiation excess and hence warming (see also figure 6).

5.2 Southern Broadleaf Forests

Broadleaf trees are also darker than grasses — albeit less so than needleleaf trees — and thus absorb excess shortwave radiation (figure 13). The only exception here is for CRCM6 during summer and fall, where incident sunlight significantly reduced by

https://doi.org/10.5194/egusphere-2022-291
Preprint. Discussion started: 10 May 2022

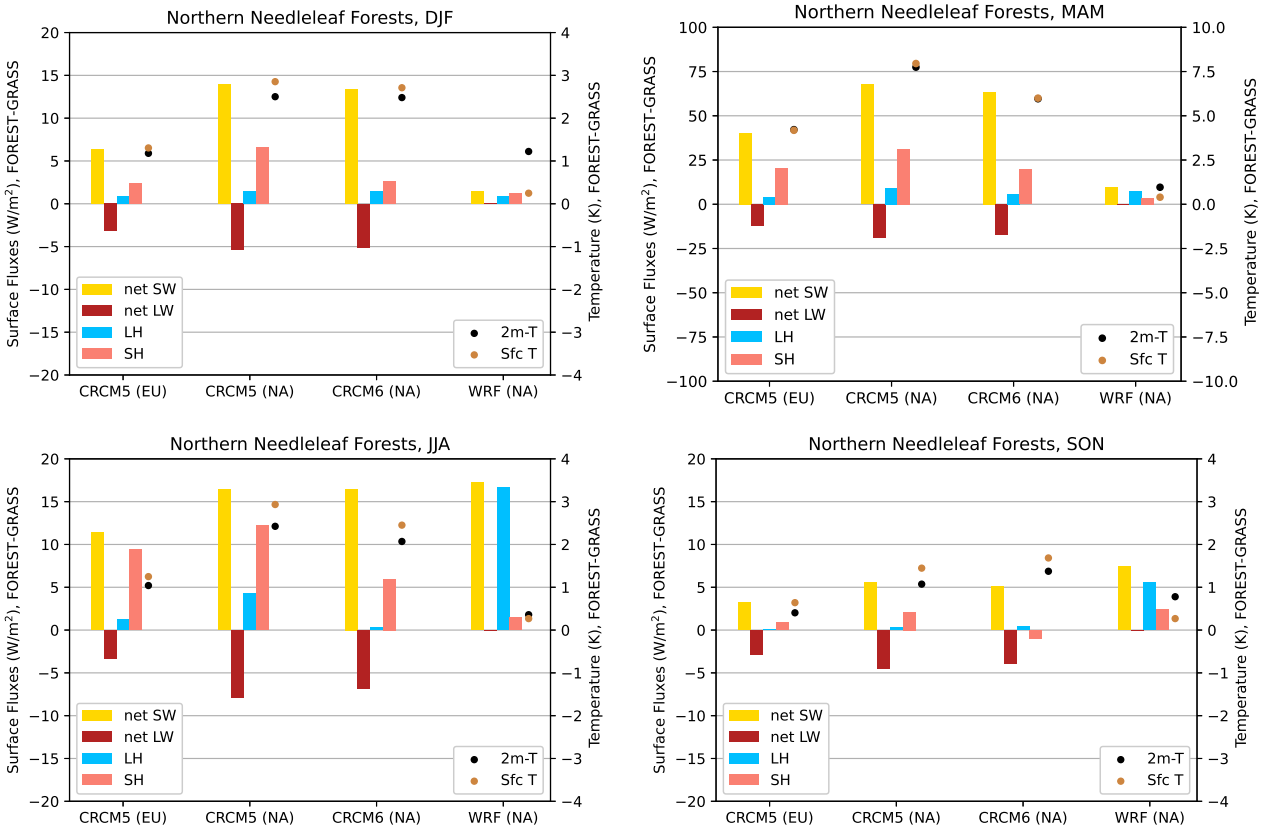

Figure 12. Surface energy fluxes breakdown over northern needleleaf forests (FOREST-GRASS). Note that the scales are blown up by factors of 2.5 and 5 for the springtime energy fluxes and temperature, respectively. Note that ground heat fluxes are not included and longwave radiation data was not available for WRF runs.

enhanced cloudiness (figure 10). This is consistent with the original LUCAS experiment (Davin et al., 2020), where forestation causes a net shortwave radiation excess in most models and seasons over France and Eastern Europe, the subdomains most similar to our southern broadleaf forest.

Compared with evergreen needleleaf forests, the energy breakdown of deciduous broadleaf forests reveals stronger seasonality. Leafless, dormant wintertime deciduous forests produce lower evapotranspiration rates less than grasses (except in WRF). But as spring comes, photosynthetically-active broadleaf trees transpire and/or intercept rain significantly more than grasses, often causing cooling in the summertime. Summer and fall surface cooling (or weak warming) are associated with the only instances of increasing net downwelling longwave radiation from forestation. That is, the cooler surface gives away less energy via infrared radiation, and/or the cloudier atmosphere radiates more of it back to the surface.

https://doi.org/10.5194/egusphere-2022-291
Preprint. Discussion started: 10 May 2022

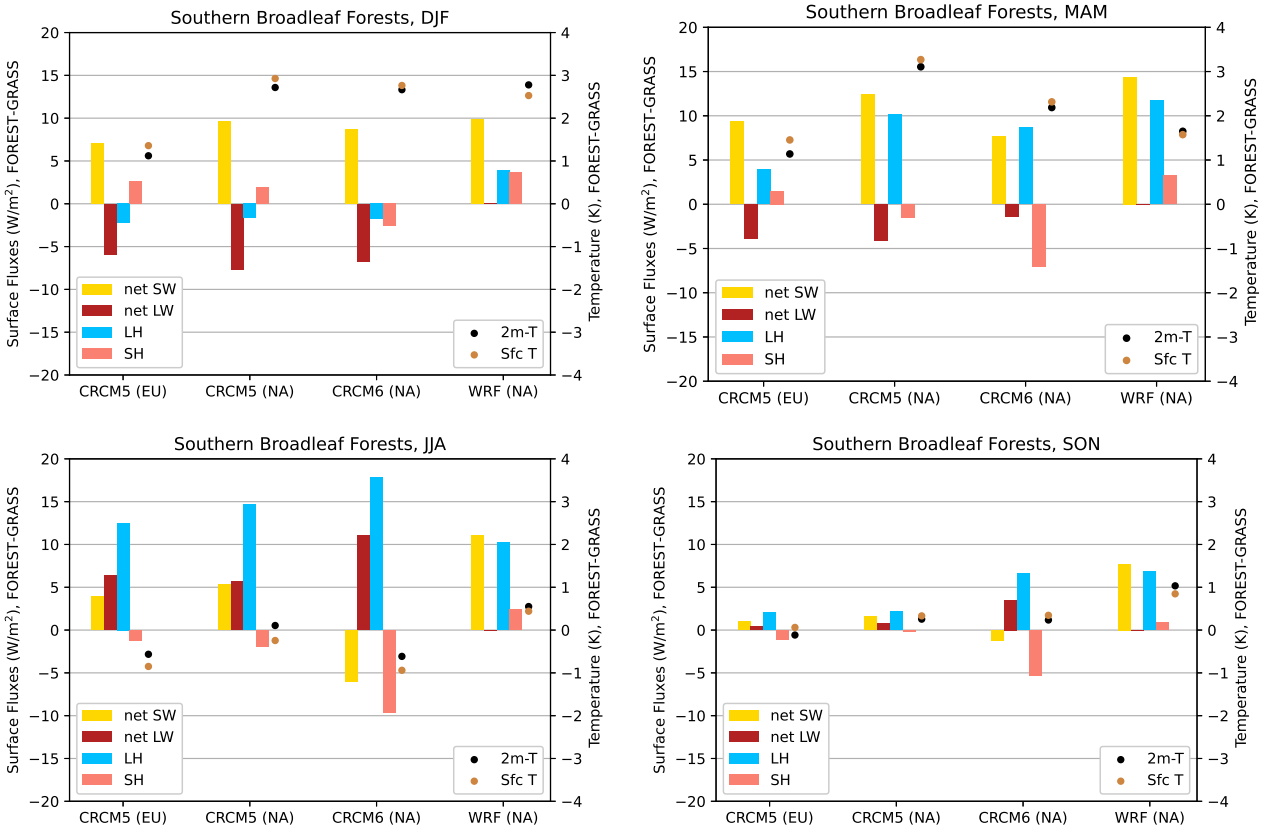

Figure 13. Surface energy fluxes breakdown over northern broadleaf forests. Following Davin et al. (2020), radiative fluxes point downward whereas turbulent fluxes point upward. Note that longwave radiation data was not available for WRF runs.

5.3 General Remarks

Despite the strong inter-model and seasonal variability in the energy breakdown, a few remarkable patterns emerge. First and foremost, the CRCM5 energy breakdown in Europe is almost always a downscaled version of its North America analog. This is true of both northern needleleaf and southern broadleaf forests. Since both forests populate lower, hence sunnier latitudes over North America (figure 1), the primary energy source of the surface is more plentiful there. As a result, forestation invariably causes more warming (or less cooling) over North America. Furthermore, how this additional energy is distributed for a given forest remains more or less unchanged across continents, echoing the similarity between the North America and Europe patterns seen in section 3. This inter-continental consistency in the CRCM5 response to forestation provides an encouraging outlook on the transferability of LUCAS results to North America.

Trees have lower albedo than grasses, an effect compounded by the snow masking of evergreen forests during winter and spring. Clouds effects aside, forestation thus creates an excess of shortwave radiation. This supplemental energy is more easily

https://doi.org/10.5194/egusphere-2022-291
Preprint. Discussion started: 10 May 2022

transferred to the atmosphere via turbulent heat fluxes because of the enhanced roughness of trees. As a result, the sum of sensible and latent heat fluxes is almost always positive in figures 12 and 13. Except for dormant wintertime leafless deciduous forests, evapotranspiration is stronger over forests than grasslands. While this is consistent with observations (Chen et al., 2018; Duveiller et al., 2018b; Meier et al., 2018; Teuling, 2018), the LUCAS ensemble reveals the opposite tendency (Davin et al., 2020).

6 Discussion and conclusions

In this paper, we present a new ensemble of regional climate simulations designed to quantify the biogeophysical effects of severe forestation. To do so, we follow the protocol outlined by Davin et al. (2020), whereby climatologies of fully afforested and deforested worlds are compared. Three regional climate models were run over North America, and one of them — CRCM5 — was also run over Europe in an attempt to bridge the gap with the original LUCAS experiment of Davin et al. (2020).

A few robust results emerge which are in line with previous model intercomparison projects, such as LUCAS and LUCID. First, trees being darker than grasses, forestation generally increases the net shortwave radiation input to the surface. Here the only exception occurs in CRCM6 during summer and fall over the eastern US, as enhanced cloudiness from heavy broadleaf evapotranspiration blocks enough sunlight to cancel the effect of reduced albedo (figure 8). In winter and spring, the albedo drop is instead compounded by the snow masking of evergreen forests in CRCMs, causing significant warming. A similar albedo-driven warming is seen over northern evergreen forests in the LUCAS experiment, with the CRCM5 producing among the strongest and most widespread of warming responses of the ensemble. We also find forestation to be associated with significant reductions in snow cover during the melting period, as in LUCAS (Mooney et al., 2021b).

Also consistent with previous investigations is the importance of turbulent fluxes partitioning for the summertime response. We find that the ratio of latent heat fluxes to the total turbulent heat fluxes, or evaporative fraction, is inversely related to the surface temperature response. While we attempt to rationalize the partition seen in our simulations using the basic vegetation parameters such as leaf area index, roughness, albedo and root depth, a robust understanding of why a given model produces a given partition is cruelly lacking, and remains an outstanding issue (Pitman et al., 2009; de Noblet-Ducoudré et al., 2012). Interestingly, even in the case of the two versions of the CRCM, which share the same land model and vegetation parameters, important differences in the turbulent fluxes partitioning are seen. We conjecture that these differences may be attributed to updates in the physics parameterizations.

What does this study teach us about the transferability of the original, European LUCAS results to North America? Encouragingly, there is strong inter-continent similarity in the CRCM5 response to forestation, which suggests that LUCAS findings may apply to North America after correcting for the differences in the vegetation distributions. One of the main findings in this paper is that both the northern needleleaf and southern broadleaf forests populating Europe and North America appear at lower, hence sunnier latitudes over the latter. It is thus to be expected that some biogeophysical effects will be magnified, as the primary energy source — sunlight — is more abundant for a given forest family.

https://doi.org/10.5194/egusphere-2022-291
Preprint. Discussion started: 10 May 2022

During winter and spring, the masking of snow by evergreen needleleaf trees reduces the surface albedo, generating excess shortwave radiation and hence warming. For a given albedo drop, the resulting warming will be proportional to the amount of sunlight received. One thus expects the wintertime warming reported in Davin et al. (2020) to be amplified over North America. This is what we see with CRCM5: the North America energy breakdown over needleleaf forests is a scaled up version of its Europe analog (figure 12). The amount of energy to spend is larger over the sunnier North America, but the way it is distributed across longwave radiation and latent and sensible heat fluxes remains unchanged.

It is important to note, however, that the simulations presented here are forced by reanalyses of the recent past (1986-2015). In a warming world, the snowline will likely retreat to higher latitudes, which would not only limit the area affected by an albedo reduction, but also move this area to less sunny regions of the globe (Diro and Sushama, 2020). One thus expects the snow-masking effect of forestation to become less potent over time.

In summertime, the large inter-model divergence both here and in previous intercomparison projects prevents any firm conclusion. We nevertheless note that broadleaf forests occupy a higher longitudinal fraction of Europe than North America, and that this is associated with a stronger, more widespread cooling spot and precipitation increase over Europe in CRCM5. Whether this inter-continental difference has robust implications would have to be checked with a larger ensemble of simulations over North America and Europe.

Echoing previous intercomparison projects, the present study emphasizes the urgency of constraining and understanding the inter-model divergence in the partition of turbulent heat fluxes. Promising avenues for confronting model output with observations are already being pursued (Duveiller et al., 2018a). In spite of these difficulties and uncertainties, this paper attests how substantial biogeophysical effects of severe forestation could be, with up to 50% changes in summertime precipitations and 10°C springtime warming simulated regionally. If anything, these results remind us that land-based mitigation strategies such as mass forestation cannot only account for carbon sequestration or albedo changes, as is usual today (Pongratz et al., 2021).

Data availability. The data and scripts used are available upon request from the corresponding author.

Author contributions. OA, MG, KW and MB produced the simulations. OA analysed the data and wrote the paper. OA, ML, DP, KW, ADL, BM and MB contributed to interpreting the results and revising the text.

Competing interests. The authors declare that they have no conflict of interest.

https://doi.org/10.5194/egusphere-2022-291
Preprint. Discussion started: 10 May 2022

Acknowledgements. Computations with the CRCM5 were carried on the SuperMUC-NG supercomputer at the Leibniz Supercomputing Centre (LRZ) of the Bavarian Academy of Sciences and Humanities. CRCM6 computations were carried on the Narval supercomputer hosted at the École de Technologie Supérieure. These computations were enabled in part by the support provided by Calcul Québec (www.calculquebec.ca) and Compute Canada (www.computecanada.ca). NCAR acknowledges high-performance computing support provided by NCAR's Computational and Information Systems Laboratory (Computational And Information Systems Laboratory, 2017). All simulations are forced using the ERA-Interim reanalysis dataset provided by the Copernicus Climate Change Service (C3S) at the European Centre for Medium-range Weather Forecast (ECMWF), available from https://www.ecmwf.int/en/forecasts/datasets/archive-datasets/reanalysis-datasets/era-interim. This material is based on work supported by NCAR, which is a major facility sponsored by the NSF under Cooperative Agreement No. 1852911. M. Bukovsky's contributions to this project were funded by the U.S. Department of Energy, Office of Science, Office of Biological and Environmental Research, Regional and Global Climate Modeling Program [grant number DE-SC0016605]. This project was made possible thanks to the funding Ouranos received from the Ministère de l'Environnement et de la Lutte contre les changements climatiques (MELCC) in support to the INFO-Crue initiative.

https://doi.org/10.5194/egusphere-2022-291
Preprint. Discussion started: 10 May 2022

References

Alexandru, A. and Sushama, L.: Impact of land-use and land-cover changes on CRCM5 climate projections over North America for the twenty-first century, Climate Dynamics, 47, 1197–1209, 2016.

Bechtold, P., Bazile, E., Guichard, F., Mascart, P., and Richard, E.: A mass-flux convection scheme for regional and global models, Quarterly Journal of the Royal Meteorological Society, 127, 869–886, 2001.

Beljaars, A. and Holtslag, A.: Flux parameterization over land surfaces for atmospheric models, Journal of Applied Meteorology and Climatology, 30, 327–341, 1991.

Betts, R. A.: Offset of the potential carbon sink from boreal forestation by decreases in surface albedo, Nature, 408, 187–190, 2000.

Blackadar, A. K.: The vertical distribution of wind and turbulent exchange in a neutral atmosphere, Journal of Geophysical Research, 67, 3095–3102, 1962.

Bourgouin, P.: A method to determine precipitation types, Weather and Forecasting, 15, 583–592, 2000.

Breil, M., Rechid, D., Davin, E., de Noblet-Ducoudré, N., Katragkou, E., Cardoso, R., Hoffmann, P., Jach, L., Soares, P., Sofiadis, G., et al.: The opposing effects of reforestation and afforestation on the diurnal temperature cycle at the surface and in the lowest atmospheric model level in the European summer, Journal of Climate, 33, 9159–9179, 2020.

Breil, M., Davin, E. L., and Rechid, D.: What determines the sign of the evapotranspiration response to afforestation in European summer?, Biogeosciences, 18, 1499–1510, 2021.

Bukovsky, M. S., Gao, J., Mearns, L. O., and O'Neill, B. C.: SSP-Based Land-Use Change Scenarios: A Critical Uncertainty in Future Regional Climate Change Projections, Earth's Future, 9, e2020EF001 782, 2021.

Chen, L., Dirmeyer, P. A., Guo, Z., and Schultz, N. M.: Pairing FLUXNET sites to validate model representations of land-use/land-cover change, Hydrology and Earth System Sciences, 22, 111–125, 2018.

Chou, M.-D. and Suarez, M. J.: An efficient thermal infrared radiation parameterization for use in general circulation models, 1994.

Côté, J., Gravel, S., Méthot, A., Patoine, A., Roch, M., and Staniforth, A.: The operational CMC–MRB global environmental multiscale (GEM) model. Part I: Design considerations and formulation, Monthly Weather Review, 126, 1373–1395, 1998.

Daloz, A. S., Schwingshackl, C., Mooney, P., Strada, S., Rechid, D., Davin, E. L., Katragkou, E., de Noblet-Ducoudré, N., Belda, M., Halenka, T., et al.: Land-atmosphere interactions in sub-polar and alpine climates in the CORDEX FPS LUCAS models: I. Evaluation of the snow-albedo effect, The Cryosphere Discussions, pp. 1–33, 2021.

Davin, E. L., Rechid, D., Breil, M., Cardoso, R. M., Coppola, E., Hoffmann, P., Jach, L. L., Katragkou, E., de Noblet-Ducoudré, N., Radtke, K., et al.: Biogeophysical impacts of forestation in Europe: first results from the LUCAS (Land Use and Climate Across Scales) regional climate model intercomparison, Earth System Dynamics, 11, 183–200, 2020.

de Noblet-Ducoudré, N., Boisier, J.-P., Pitman, A., Bonan, G., Brovkin, V., Cruz, F., Delire, C., Gayler, V., Van den Hurk, B., Lawrence, P., et al.: Determining robust impacts of land-use-induced land cover changes on surface climate over North America and Eurasia: Results from the first set of LUCID experiments, Journal of Climate, 25, 3261–3281, 2012.

Dee, D. P., Uppala, S. M., Simmons, A. J., Berrisford, P., Poli, P., Kobayashi, S., Andrae, U., Balmaseda, M., Balsamo, G., Bauer, d. P., et al.: The ERA-Interim reanalysis: Configuration and performance of the data assimilation system, Quarterly Journal of the royal meteorological society, 137, 553–597, 2011.

Delage, Y.: Parameterising sub-grid scale vertical transport in atmospheric models under statically stable conditions, Boundary-Layer Meteorology, 82, 23–48, 1997.

https://doi.org/10.5194/egusphere-2022-291
Preprint. Discussion started: 10 May 2022

Diro, G. and Sushama, L.: Contribution of snow cover decline to projected warming over North America, Geophysical Research Letters, 47, e2019GL084 414, 2020.

Duveiller, G., Forzieri, G., Robertson, E., Li, W., Georgievski, G., Lawrence, P., Wiltshire, A., Ciais, P., Pongratz, J., Sitch, S., et al.: Biophysics and vegetation cover change: a process-based evaluation framework for confronting land surface models with satellite observations, Earth System Science Data, 10, 1265–1279, 2018a.

Duveiller, G., Hooker, J., and Cescatti, A.: The mark of vegetation change on Earth's surface energy balance, Nature communications, 9, 1–12, 2018b.

Girard, C., Plante, A., Desgagné, M., McTaggart-Cowan, R., Côté, J., Charron, M., Gravel, S., Lee, V., Patoine, A., Qaddouri, A., et al.: Staggered vertical discretization of the Canadian Environmental Multiscale (GEM) model using a coordinate of the log-hydrostatic-pressure type, Monthly Weather Review, 142, 1183–1196, 2014.

Hong, S.-Y., Dudhia, J., and Chen, S.-H.: A revised approach to ice microphysical processes for the bulk parameterization of clouds and precipitation, Monthly weather review, 132, 103–120, 2004.

Jach, L., Warrach-Sagi, K., Ingwersen, J., Kaas, E., and Wulfmeyer, V.: Land Cover Impacts on Land-Atmosphere Coupling Strength in Climate Simulations With WRF Over Europe, Journal of Geophysical Research: Atmospheres, 125, e2019JD031 989, 2020.

Jach, L., Schwitalla, T., Branch, O., Warrach-Sagi, K., and Wũlfmeyer, V.: Sensitivity of land–atmosphere coupling strength to changing atmosphe ric temperature and moisture over Europe, Earth System Dynamics, 13, 109–132, https://doi.org/10.5194/esd-13-109-2022, 2022.

Jacob, D., Petersen, J., Eggert, B., Alias, A., Christensen, O. B., Bouwer, L. M., Braun, A., Colette, A., Déqué, M., Georgievski, G., et al.: EURO-CORDEX: new high-resolution climate change projections for European impact research, Regional environmental change, 14, 563–578, 2014.

Janjić, Z. I.: The step-mountain eta coordinate model: Further developments of the convection, viscous sublayer, and turbulence closure schemes, Monthly weather review, 122, 927–945, 1994.

Kain, J. S.: The Kain–Fritsch convective parameterization: an update, Journal of applied meteorology, 43, 170–181, 2004.

Kain, J. S. and Fritsch, J. M.: A one-dimensional entraining/detraining plume model and its application in convective parameterization, Journal of Atmospheric Sciences, 47, 2784–2802, 1990.

Kuo, H.-L.: On formation and intensification of tropical cyclones through latent heat release by cumulus convection, Journal of the atmospheric sciences, 22, 40–63, 1965.

Lawrence, P. J. and Chase, T. N.: Representing a new MODIS consistent land surface in the Community Land Model (CLM 3.0), Journal of Geophysical Research: Biogeosciences, 112, 2007.

Lejeune, Q., Seneviratne, S. I., and Davin, E. L.: Historical land-cover change impacts on climate: Comparative assessment of LUCID and CMIP5 multimodel experiments, Journal of Climate, 30, 1439–1459, 2017.

Li, J. and Barker, H.: A radiation algorithm with correlated-k distribution. Part I: Local thermal equilibrium, Journal of the atmospheric sciences, 62, 286–309, 2005.

Li, W., Li, L., Chen, J., Lin, Q., and Chen, H.: Impacts of land use and land cover change and reforestation on summer rainfall in the Yangtze River basin, Hydrology and Earth System Sciences, 25, 4531–4548, 2021.

Li, Y., Zhao, M., Motesharrei, S., Mu, Q., Kalnay, E., and Li, S.: Local cooling and warming effects of forests based on satellite observations, Nature communications, 6, 1–8, 2015.

https://doi.org/10.5194/egusphere-2022-291
Preprint. Discussion started: 10 May 2022

Martynov, A., Laprise, R., Sushama, L., Winger, K., Šeparović, L., and Dugas, B.: Reanalysis-driven climate simulation over CORDEX North America domain using the Canadian Regional Climate Model, version 5: model performance evaluation, Climate Dynamics, 41, 2973–3005, 2013.

McTaggart-Cowan, R., Vaillancourt, P., Zadra, A., Chamberland, S., Charron, M., Corvec, S., Milbrandt, J., Paquin-Ricard, D., Patoine, A., Roch, M., et al.: Modernization of atmospheric physics parameterization in Canadian NWP, Journal of Advances in Modeling Earth Systems, 11, 3593–3635, 2019.

Mearns, L. O., Arritt, R., Biner, S., Bukovsky, M. S., McGinnis, S., Sain, S., Caya, D., Correia, J., Flory, D., Gutowski, W., et al.: The North American regional climate change assessment program: overview of phase I results, Bulletin of the American Meteorological Society, 93, 1337–1362, 2012.

Meier, R., Davin, E. L., Lejeune, Q., Hauser, M., Li, Y., Martens, B., Schultz, N. M., Sterling, S., and Thiery, W.: Evaluating and improving the Community Land Model's sensitivity to land cover, Biogeosciences, 15, 4731–4757, 2018.

Mlawer, E. J., Taubman, S. J., Brown, P. D., Iacono, M. J., and Clough, S. A.: Radiative transfer for inhomogeneous atmospheres: RRTM, a validated correlated-k model for the longwave, Journal of Geophysical Research: Atmospheres, 102, 16 663–16 682, 1997.

Mooney, P., Sobolowski, S., and Lee, H.: Designing and evaluating regional climate simulations for high latitude land use land cover change studies, Tellus A: Dynamic Meteorology and Oceanography, 72, 1–17, 2020.

Mooney, P., Lee, H., and Sobolowski, S.: Impact of Quasi-Idealized Future Land Cover Scenarios at High Latitudes in Complex Terrain, Earth's Future, 9, e2020EF001 838, 2021a.

Mooney, P. A., Rechid, D., Davin, E. L., Katragkou, E., de Noblet-Ducoudré, N., Breil, M., Cardoso, R. M., Daloz, A. S., Hoffmann, P., Lima, D. C., et al.: Land-atmosphere interactions in sub-polar and alpine climates in the CORDEX FPS LUCAS models: Part II. The role of changing vegetation, The Cryosphere Discussions, pp. 1–22, 2021b.

Perugini, L., Caporaso, L., Marconi, S., Cescatti, A., Quesada, B., de Noblet-Ducoudre, N., House, J. I., and Arneth, A.: Biophysical effects on temperature and precipitation due to land cover change, Environmental Research Letters, 12, 053 002, 2017.

Pitman, A. J., de Noblet-Ducoudré, N., Cruz, F., Davin, E. L., Bonan, G., Brovkin, V., Claussen, M., Delire, C., Ganzeveld, L., Gayler, V., et al.: Uncertainties in climate responses to past land cover change: First results from the LUCID intercomparison study, Geophysical Research Letters, 36, 2009.

Pongratz, J., Schwingshackl, C., Bultan, S., Obermeier, W., Havermann, F., and Guo, S.: Land Use Effects on Climate: Current State, Recent Progress, and Emerging Topics, Current Climate Change Reports, pp. 1–22, 2021.

Roe, S., Streck, C., Obersteiner, M., Frank, S., Griscom, B., Drouet, L., Fricko, O., Gusti, M., Harris, N., Hasegawa, T., et al.: Contribution of the land sector to a 1.5 C world, Nature Climate Change, 9, 817–828, 2019.

Šeparović, L., Alexandru, A., Laprise, R., Martynov, A., Sushama, L., Winger, K., Tete, K., and Valin, M.: Present climate and climate change over North America as simulated by the fifth-generation Canadian regional climate model, Climate Dynamics, 41, 3167–3201, 2013.

Shukla, P., Skea, J., Calvo Buendia, E., Masson-Delmotte, V., Pörtner, H., Roberts, D., Zhai, P., Slade, R., Connors, S., Van Diemen, R., et al.: IPCC, 2019: Climate Change and Land: an IPCC special report on climate change, desertification, land degradation, sustainable land management, food security, and greenhouse gas fluxes in terrestrial ecosystems, 2019.

Skamarock, W. C., Klemp, J. B., Dudhia, J., Gill, D. O., Barker, D. M., Wang, W., and Powers, J. G.: A description of the advanced research WRF version 2, Tech. rep., National Center For Atmospheric Research Boulder Co Mesoscale and Microscale . . . , 2005.

https://doi.org/10.5194/egusphere-2022-291
Preprint. Discussion started: 10 May 2022

Sofiadis, G., Katragkou, E., Davin, E. L., Rechid, D., de Noblet-Ducoudre, N., Breil, M., Cardoso, R. M., Hoffmann, P., Jach, L., Meier, R., et al.: Afforestation impact on soil temperature in regional climate model simulations over Europe, Geoscientific Model Development Discussions, pp. 1–35, 2021.

Solman, S. A., Sanchez, E., Samuelsson, P., da Rocha, R. P., Li, L., Marengo, J., Pessacg, N. L., Remedio, A., Chou, S., Berbery, H., et al.: Evaluation of an ensemble of regional climate model simulations over South America driven by the ERA-Interim reanalysis: model performance and uncertainties, Climate Dynamics, 41, 1139–1157, 2013.

Sundqvist, H., Berge, E., and Kristjánsson, J. E.: Condensation and cloud parameterization studies with a mesoscale numerical weather prediction model, Monthly Weather Review, 117, 1641–1657, 1989.

Teuling, A. J.: A forest evapotranspiration paradox investigated using lysimeter data, Vadose Zone Journal, 17, 1–7, 2018.

Verseghy, D., McFarlane, N., and Lazare, M.: CLASS—A Canadian land surface scheme for GCMs, II. Vegetation model and coupled runs, International journal of climatology, 13, 347–370, 1993.

Verseghy, D. L.: CLASS—A Canadian land surface scheme for GCMs. I. Soil model, International Journal of Climatology, 11, 111–133, 1991.

Windisch, M. G., Davin, E. L., and Seneviratne, S. I.: Prioritizing forestation based on biogeochemical and local biogeophysical impacts, Nature Climate Change, 11, 867–871, 2021.

https://doi.org/10.5194/egusphere-2022-291
Preprint. Discussion started: 10 May 2022

Model name	WRF	CRCM5	CRCM6
Institution	NCAR	Ouranos	UQAM
Land Surface Scheme	Unified NOAH	CLASS v3.5c	CLASS v3.6
Land cover classes (principal classes used in FOREST or GRASS are in **bold**, classes used but with a minor impact are *italiziced*)	1: Urban and Built-up Land 2: Dryland Cropland and Pasture 3: Irrigated Cropland and Pasture 4: Mixed Dryland/Irrigated Cropland and Pasture 5. Cropland/Grassland Mosaic 6. Cropland/Woodland Mosaic **7. Grassland** 8. Shrubland 9. Mixed Shrubland/Grassland 10. Savanna **11. Deciduous Broadleaf Forest** *12. Deciduous Needleleaf Forest* *13. Evergreen Broadleaf* **14. Evergreen Needleleaf** 15. Mixed Forest **16. Water Bodies** 17. Herbacious Wetland 18. Wooden Wetland *19. Barren or Sparlsely Vegetated* 20. Herbaceous Tundra 21. Wooded Tundra 22. Mixed Tundra 23. Bare Ground Tundra **24. Snow or Ice**	**1: Evergreen Needleleaf Trees** *2: Evergreen Broadleaf Trees* *3: Deciduous Needleleaf Trees* **4: Deciduous Broadleaf Trees** 5: Tropical Broadleaf Trees 6: Drought Deciduous Trees 7: Evergreen Broadleaf Shrub 8: Deciduous Shrubs 9: Thorn Shrubs **10: Short Grass & Forbs** 11: Long Grass 12: Crops 13: Rice 14: Sugar 15: Maize 16: Cotton 17: Irrigated Crops 18: Urban 19: Tundra 20: Swamp **21: Desert** 22: Mixed Wood Forests 23: Mixed Shrubs	**1: Evergreen Needleleaf Trees** *2: Evergreen Broadleaf Trees* *3: Deciduous Needleleaf Trees* **4: Deciduous Broadleaf Trees** 5: Tropical Broadleaf Trees 6: Drought Deciduous Trees 7: Evergreen Broadleaf Shrub 8: Deciduous Shrubs 9: Thorn Shrubs **10: Short Grass & Forbs** 11: Long Grass 12: Crops 13: Rice 14: Sugar 15: Maize 16: Cotton 17: Irrigated Crops 18: Urban 19: Tundra 20: Swamp **21: Desert** 22: Mixed Wood Forests 23: Mixed Shrubs
Conversion method to implement the vegetation maps (FOREST and GRASS)	bare soil = 19 Needleleaf Evergreen Temperate = 14 Needleleaf Evergreen Boreal = 14 Needleleaf Deciduous Boreal = 12 Broadleaf Evergreen Tropical = 13 Broadleaf Evergreen Temperate = 13 Broadleaf Deciduous Tropical = 11 Broadleaf Deciduous Temperate = 11 Broadleaf Deciduous Boreal = 11 C3 Arctic Grass = 7 C3 Grass = 7 C4 Grass = 7	bare soil = 21 Needleleaf Evergreen Temperate = 1 Needleleaf Evergreen Boreal = 1 Needleleaf Deciduous Boreal = 3 Broadleaf Evergreen Tropical = 2 Broadleaf Evergreen Temperate = 2 Broadleaf Deciduous Tropical = 4 Broadleaf Deciduous Temperate = 4 Broadleaf Deciduous Boreal = 4 C3 Arctic Grass = 10 C3 Grass = 10 C4 Grass = 10	bare soil = 21 Needleleaf Evergreen Temperate = 1 Needleleaf Evergreen Boreal = 1 Needleleaf Deciduous Boreal = 3 Broadleaf Evergreen Tropical = 2 Broadleaf Evergreen Temperate = 2 Broadleaf Deciduous Tropical = 4 Broadleaf Deciduous Temperate = 4 Broadleaf Deciduous Boreal = 4 C3 Arctic Grass = 10 C3 Grass = 10 C4 Grass = 10
Representation of sub-grid scale vegetation heterogeneity	The dominant class sets the surface properties, other class properties ignored	The surface properties are averaged over the different classes present on a given tile	The surface properties are averaged over the different classes present on a given tile
Leaf area index	Estimated using seasonally varying green vegetation coverage fraction (FVEG) and the minimum and maximum values for LAI (LAIMIN and LAIMAX, respectively) prescribed for each vegetation type. LAI=((1.0-FVEG)*LAIMIN)+(FVEG*LAIMAX)	Seasonal cycle with the onset of spring budburst and fall senescence triggered by near-zero values of the air temperature and the first soil layer temperature.	Seasonal cycle with the onset of spring budburst and fall senescence triggered by near-zero values of the air temperature and the first soil layer temperature.
Total soil depth and number of hydrologically/thermally active soil layers	4 thermally and hydrologically active soil layers with a maximum depth of 2m	17 thermally and hydrologically active soil layers with maximum depth of 5m.	17 thermally and hydrologically active soil layers with maximum depth of 5m.
Initialization and spin-up	Initialization with ERA-Interim	Initialization with ERA-Interim	Initialization with ERA-Interim
Lateral boundary formulation	linear relaxation	10 semi-lag departure points	10 semi-lag departure points
Buffer (no. of grid cells)	5	20 grid cells lateral sponge zone	grid cells lateral sponge zone: 10 in longitude, 15 in latitude
No. of vertical levels	28	56	71
Turbulence and planetary boundary layer scheme	MYJ (Janjić 1994)	1.5-order closure based on prognostic turbulence kinetic energy (Bélair et al. 1999). Mixing length based on Bougeault and Lacarrère (1989). Stability functions from Delage (1997)	1.5-order closure based on prognostic turbulence kinetic energy (Bélair et al. 1999). Mixing length based on Bougeault and Lacarrère (1989), except in laminar conditions where Blackadar (1962) is used. Stability functions from Beljaars and Holtslag (1991).
Radiation scheme	Longwave: RRTM (Mlawer et al. 1997); Shortwave: Goddard (Chou and Suarez 1994)	Li & Baker (2015)	Li & Baker (2015), with a few updates described in McTaggart et al. (2019)
Deep Convection scheme	Kain-Fritsch w/ ETA trigger (Kain 2004)	Kain & Fritsch (1990)	Kain & Fristch (1990), with a few updates described in McTaggart et al. (2019)
Shallow Convection scheme	n/a	Kuo (1965) transient	Bechtold (2001)
Microphysics scheme	WSM3 (Hong et al. 2004)	modified Sundqvist (1989); Bourgouin (2000)	modified Sundqvist (1989); Bourgouin (2000)
Greenhouse gases	Historical	Historical + RCP4.5	Historical + RCP8.5
Aerosols	Prescribed Observed, Uniform	Prescribed Observed	Hardcoded: higher values ove land than ove ocean; higher values at the equator than at the poles

Table 1. Main properties of the models used in this paper. See table 1 from Davin et al. (2020) for comparison with the original LUCAS ensemble.

https://doi.org/10.5194/egusphere-2022-291
Preprint. Discussion started: 10 May 2022

CRCM-CLASS	Needleleaf	Broadleaf	Grasses
Min. Stomatal Resistance (s/m)	250	130	150
Albedo (visible/near-IR)	0.03/0.19	0.05/0.29	0.05/0.31
LAI (min - max)	1.6 - 2	0.5 - 6	4
Root Depth (m)	1	2	1.2
Roughness Length (m)	1.5	2	0.08

WRF-NOAH	Needleleaf	Broadleaf	Grasses
Min. Stomatal Resistance (s/m)	125	100	40
Albedo (min - max)	0.12	0.16 - 0.17	0.19 - 0.23
LAI (min - max)	5 - 6.4	1.85 - 3.31	0.52 - 2.90
Root Depth (n layers)	4	4	3
Roughness Length (m)	0.5	0.5	0.1

Table 2. Principal parameters of the main land categories used in CLASS and in NOAH (bold font in table 1). Minimum and maximum values for leaf area index (LAI) and albedo are tied to the seasonal cycle.